Supplementary material

Aerosol opto-physical properties: Temporal variation, aerosol type discrimination and source identification

A.R. Kolhe[1], G.R. Aher[2,*], P.S. Soyam[3,6], S.D. Ralegankar[4], S. Kedia[5], L.M. Chaudhari[2], V.V. Antad[2], S.D. Ghude[6], P.D. Safai[6], S.D. Chakane[1], P.C.S. Devara[7]

[1]Department of Physics, Arts, Science and Commerce College, Indapur, Pune, India
[2]Department of Physics, Nowrosjee Wadia College, Pune, India
[3]Department of Environmental Sciences, Savitribai Phule Pune University, Pune, India
[4]Department of Physics, Ahmednagar College, Ahmednagar, India
[5]Center for Development of Advanced Computing, Pune, India
[6]Indian Institute of Tropical Meteorology, Pashan, Pune, India
[7]Amity Centre for Ocean-Atmospheric Science and Technology, Amity University Haryana, India

*Corresponding Author: Dr. G. R. Aher
E-mail address: aher.g.r@gmail.com

(A) DATA, INSTRUMENTATION, AND ANALYSIS TECHNIQUE

Calibration of Microtops II Sun photometer

It is required to calibrate Sun photometers/multiple wavelengths solar radiometers at the pristine, mountain observational site (Ningombam et al., 2014; Dumka et al., 2020) having stable atmospheric conditions so that spectral optical excitation remains nearly same throughout the observing day. In the present work, the Microtops II Sun photometer has been calibrated at the mountain site Mt. Sinhagad situated to the North- West of Pune. During the calibration campaign, Microtops II sun photometer was operated at different optical air masses throughout the day under practically stable atmospheric and pristine sky conditions and Langley plots (a plot of signal voltage $\ln V(\lambda)$ against relative optical air mass) at 440, 500, 675, 870 and 1020 nm wavelengths were constructed. From these plots (Fig. S1), the ordinate intercept, $\ln V_0(\lambda)$ for each wavelength was determined by subjecting each Langley plot to linear

regression technique and the statistical metrics of each Langley plot are listed in Table S1. It is seen that at all the wavelength channels the magnitude of $\ln V_0$ is found to be significantly less than 1% which highlights the stability of the instrument for AOD measurements (Table S1).

(B) RESULTS AND DISCUSSION

(i) Spectral variation of AOD

Spectral AOD is an essential parameter in determining the extent to which aerosols directly perturb the Earth-atmosphere radiation budget. It is found to depend on their columnar distribution, size spectrum, and refractive index (Pawar et al., 2012; Varpe et al., 2018). Fig.S1 shows the average AOD spectra over the site AC-Ahmednagar in winter and pre-monsoon seasons. As seen in Fig. S1, the length of vertical bars shows larger to smaller variation in AODs from shorter to longer wavelengths respectively during both seasons. The relatively strong wavelength dependence of AOD is evident in Fig. S1, which illustrates that AOD is higher at shorter wavelengths ($\lambda < 0.6$ μm). AOD gradually decreases towards longer wavelengths ($\lambda > 0.6$ μm) despite seasonal change attributed to the dominance of the fine-mode aerosols over coarse-mode aerosols at the observing site. Moreover, the spectral dependence of AOD is found to be decay type indicating the possibility of a similar kind of aerosol particle size distribution albeit variation in their columnar content based on AOD magnitude at each wavelength (More et al., 2013). According to Mie scattering theory (Quenzel et al., 1970), the occurrence of a higher columnar concentration of fine-mode aerosols in the atmosphere over the observing site cause wavelength-selective scattering of the solar irradiance producing higher AODs at the shorter wavelengths. Similarly, the coarse-mode aerosols provide likewise contributions to the AOD at both wavelengths (Schuster et al., 2006). In the multi-wavelength radiometer (MWR) studies over Dehradun (30°00’ N – 30°30’ N and 78°18’ E – 78°36’ E), Rana et al. (2009) have found

similar AOD spectral dependence during the pre-monsoon as well as the winter seasons as is reported in the present work. Ranjan et al. (2007) have reported spectral AOD measurements over Rajkot by employing Microtops II Sunphotometer during March 2005–March 2006. Their results portrayed AOD seasonal variations with high/low AODs in pre-monsoon/winter seasons. The study also reveals more AOD decrease at higher wavelengths as a consequence of the reduction in coarse-mode aerosols in the winter season while the AOD amplitude at longer wavelengths is seen to be higher during pre-monsoon season showing the substantial contribution of coarse-mode aerosols over fine-mode aerosols. The occurrence of high AODs at larger wavelengths during pre-monsoon season could be assigned to the dominance of coarse-mode particles due to prominent surface wind activity which causes lifting-up of the soil-dust from the dry surface into the atmosphere and the long-range transported mineral-dust from arid regions (Aher et al., 2014; Pawar et al., 2015). During the winter season, the frequency of the strong nocturnal inversions is normally high (Vernekar et al., 1993). Aerosols produced due to anthropogenic activities (e.g., vehicular emissions, domestic cooking, industrial emissions, etc.) are released into the surface layers and get trapped in the ABL due to less atmospheric ventilation (Kolhe et al., 2018). Further, the concentration of the soil dust aerosols is less during winter on account of calm weather conditions. As a result of this, AODs are comparatively higher at shorter wavelengths during winter as compared to those observed in the pre-monsoon season (Dani et al., 2012).

Beegum et al. (2008) have identified the impact of long-range advection of aerosols from the adjoining areas resulting in the significant variations in the AOD magnitudes and their wavelength dependence measured during March to May 2006 in the Integrated Campaigns for Aerosols, gases, and Radiation Budget (ICARB). Also, picking of dust aerosols by the prominent

convective eddies caused by the strong heating of the land surface (a meso-scale mechanism) could be the plausible reason behind the modulation of the observed AOD and its spectral variability (Moorthy et al., 2007).

(ii) Comparison of Microtops II Sunphotometer measured and MODIS retrieved AODs

The comparison of the ground-based AOD measurements with those retrieved from the satellite-based observations and thereby the assessment of satellite aerosol product retrievals has major theoretical as well as practical implications in the up-gradation of the retrieval algorithms and in climate research. The MODerate resolution Imaging Spectroradiometer (MODIS) onboard Terra/Aqua satellite provides spectral information of aerosol parameters in the mid-visible wavelength region. Terra/Aqua satellites are operated at 705 km altitude with an equator crossing time of about 10:30/13:30 hr (IST). Recently, many researchers have performed clear and extensive studies on the validation of MODIS aerosol products (Chu et al., 2002; Ichokuet al., 2002; Levy et al., 2005, 2010; Bennouna et al., 2011; Bibi et al., 2015; Ma et. al., 2016; Vijayakumar et al., 2016; Ali et al., 2017; Wang et al., 2017a, 2017b; Boiyo et al., 2017; Gupta et al., 2018; Tian and Gao, 2019; Sharma et al., 2021). It is crucial for the individual researcher to choose MODIS retrieved aerosol products comprising of the realistic results based on the quantitative analysis of aerosol data and the comparison of different MODIS retrieved aerosol products. For comparison, MODIS retrieved AODs require to be spatio-temporally collocated with Microtops II AOD measurements. The collocation is needed since the MODIS sensor scan encompasses spatial coverage of the study area from the space whereas Microtops II is a ground-based point measurement. The objective of the spatio-temporal collocation process is to co-locate the air mass perceived by the MODIS sensor from

the space over the study location, which is concurrently observed by the ground-based Microtops II sensor. In the present study, the comparison of the Terra platform MODIS sensor DT-DB combined algorithm retrieved AOD (MOD04_3K_C6.1 (collection 6.1) retrieved from https://ladsweb.modaps.eosdis.nasa.gov/) is attempted by comparing it with ground-based Microtops II Sun photometer derived AOD data at the same wavelength. For achieving the realistic comparison between Microtops II and MODIS AODs, AODs for Microtops II at 550 nm has calculated by using the Ångström empirical formula (Eq. S1)

$$AOD_{550\,nm} = AOD_{500\,nm} \times \left(\frac{550}{500}\right)^{-AE} \quad \text{(S1)}$$

where, AE is the Ångström exponent estimated by employing linear regression technique to spectral AOD curve in the 440–870 nm spectral range (Pawar et al., 2015). The validation process consists of plotting of the collocated MODIS/Terra and Microtops II AODs on a 2-D scatter diagram and performing linear regression fit to the plotted data (More et al., 2013; Sayer et al., 2014; Wang et al., 2017a, 2017b; Boiyo et al., 2017; Sharma et al., 2021). Here, the scatter diagram of the Microtops II calculated $AOD_{550\,nm}$ against MODIS/Terra Dark Target-Deep Blue combined (DT-DB) retrieved $AOD_{550\,nm}$ is constructed and is shown in Fig. S3. The expected error (EE) envelope, determined from the MODIS/Terra 3-km DT/DB combined product over Land and Ocean, representing the percentages of the AOD retrievals falling within/above/below (PWE/PAE/PBE) the custom error range, is determined by employing Eq. (S2),

$$EE = \pm(0.05 + 0.15 * AOD_{Microtops}) \quad \text{(S2)}$$

The regression line is represented by the red solid line, the blue and green solid lines are above and below EE bounds respectively, and the black dashed line indicates the X = Y line. The estimated y-intercepts and slopes for linear regression analysis are given in Eq. (S3),

$$AOD_{MODIS} = \left[AOD_{MicrotopsII} \times (1.09 \pm 0.05)\right] + (-0.01 \pm 0.02) \quad \text{(S3)}$$

In this study, the following statistical parameters are used to quantitatively evaluate the consistency and uncertainty that may be prevalent in the Microtops-II and MODIS/Terra AOD retrievals: the Pearson's correlation coefficient (r), the coefficient of determination (R^2), the mean absolute/absolute percentage error (MAE, Eq. (S4)), the root-mean-square error (RMSE, Eq. (S5)), and the relative mean bias (RMB, Eq. (S6)).

$$MAE = \frac{1}{n}\sum_{i=1}^{n}\left|AOD_{(MODIS)i} - AOD_{(Microtops)i}\right| \quad \text{(S4)}$$

$$RMSE = \sqrt{\frac{1}{n}\sum_{i=1}^{n}\left(AOD_{(MODIS)i} - AOD_{(Microtops)i}\right)^2} \quad \text{(S5)}$$

$$RMB = \frac{\overline{AOD_{MODIS}}}{\overline{AOD_{Microtops}}} \quad \text{(S6)}$$

As noticed from Fig. S3, the MODIS C6.1 DT-DB combined AODs depict a high correlation (r = 0.87, slope = 1.09 ± 0.05, RMSE = 0.08 and RMB = 1.06 with low MAE = 0.06) with Microtops ground measurements and very high accuracy (PWE = 82.7%), which is higher than the average global level (66%, Levy et al., 2010). Also, the figure demonstrates a significant overestimation over the study region with RMB (1.06) greater than 1.0, and PAE (11.3%) values. Significant overestimation in MODIS/Terra AOD retrievals in the presence of low and high aerosol loadings may be produced due to the errors in instrument calibration, surface reflectance assumptions, and aerosol models used for aerosol inversion algorithm (More et al., 2013; Sharma

et al., 2021). Also, mixing with non-absorbing fine mode aerosols from urban pollution (results in over-prediction of absorption) over AC-Ahmednagar may be one of the causes of overestimation of MODIS/Terra AOD (Nichol and Bilal, 2016). The estimated linear regression fit parameters viz., slope, intercept, r, and R^2 of the fit reveal a close agreement between AODs from Microtops II and MODIS/Terra.

REFERENCES

Aher, G.R., Pawar, G.V., Gupta, P., Devara, P.C.S. (2014). Effect of Major Dust Storm on Optical, Physical, and Radiative Properties of Aerosols over Coastal and Urban Environments in Western India. Int. J. Remote Sens. 35, 871–903. Doi:10.1080/01431161.2013.873153.

Ali, M.A., Assiri, M., Dambul, R. (2017). Seasonal aerosol optical depth (AOD) variability using satellite data and its comparison over Saudi Arabia for the period 2002–2013. Aerosol Air Qual. Res.17, 1267–1280. Doi: 10.4209/aaqr.2016.11.0492.

Beegum S.N., Moorthy, K.K., Nair, V.S., Babu, S.S., Satheesh, S.K., Vinoj, V., Reddy R.R., Rama Gopal, K., Badarinath, K.V.S., Niranjan, K., Pandey, S.K., Behera, M., Jayaraman, A., Bhuyan, P.K., Gogoi, M.M., Singh, S., Pant, P., Dumka, U.C., Kant, Y., Kuniyal, J.C., Singh, D. (2008). Characteristics of spectral aerosol optical depths over India during ICARB. J. Earth Syst. Sci. 117 (S1), 303–313.

Bennouna, Y.S., Cachorro, V.E., Toledano, C., Berjón, A., Prats, N., Fuertes, D., Gonzalez, R., Torres, B., De Frutos, A.M. (2011). Comparison of atmospheric aerosol climatologies over southwestern Spain derived from AERONET and MODIS. Remote Sens. Environ.115, 1272 – 1284. http://dx.doi.org/10.1016/j.rse.2011.01.011.

Bibi, H., Khan, A., Chishtie, F., Bibi, S., Shahid, I., Blaschke, T. (2015). Intercomparison of MODIS, MISR, OMI, and CALIPSO aerosol optical depth retrievals for four locations on the Indo-Gangetic plains and validation against AERONET data. Atmos. Environ. 111,113–126.

Boiyo, R., Kumar, K.R., Zhao, T. (2017). Statistical intercomparison and validation of multisensory aerosol optical depth retrievals over three AERONET sites in Kenya, East Africa. Atmos. Res. 197,277–288.

Chu, D.A., Kaufman, Y.J., Ichoku, C., Remer, L.A., Tanre, D., Holben, B.N. (2002). Validation of MODIS aerosol optical depth retrieval over land. Geophys. Res. Lett. 29 (12), 1617, Doi: 10.1029/2001GL013205.

Dani, K.K., Ernest Raj, P., Devara, P.C.S., Pandithurai, G., Sonbawne, S.M., Maheskumar, R.S., Saha, S.K., Jaya Rao, Y. (2012). Long-term trends and variability in measured multi-spectral aerosol optical depth over a tropical urban station in India. Int. J. Climatol. 32, 153–160. Doi:10.1002/joc.2250.

Dumka, U.C., Ningombam, S. S., Kaskaoutis, D.G., Madhavan, B.L., Song, H.-J., Angchuk, D., Jorphail, S. (2020). Long-term (2008–2018) aerosol properties and radiative effect at high-altitude sites over western trans-Himalayas, Sci. Total Environ. 734, 139354.

Gupta, P., Remer, L.A., Levy, R.C., Mattoo, S. (2018). "Validation of MODIS 3 km land aerosol optical depth from NASA's EOS Terra and Aqua missions". Atmospheric Measurement Techniques, 11: 3145–3159. doi: 10.5194/amt-11-3145-2018.

Ichoku, C., Chu, D.A., Mattoo, S., Kaufman, Y.J., Remer, L.A., Tanre, D., Slutsker, I., Holben, B.N. (2002). A spatio-temporal approach for global validation and analysis of MODIS aerosol products. Geophys. Res. Lett. 29 (12), 1616. Doi:10.1029/2001GL013206.

Kolhe, A.R., Aher, G.R., Ralegankar, S.D., Safai, P.D. (2018). Investigation of aerosol black carbon over semi-urban and urban locations in south-western India. Atmos. Pollution Res. 9, 1111–1130. Doi:10.1016/j.apr.2018.04.010.

Levy, R.C., Remer, L.A., Kleidman, R.G., Mattoo, S., Ichoku, C., Kahn, R., Eck, T.F. (2010). Global evaluation of the collection 5 MODIS dark-target aerosol products overland. Atmos. Chem. Phys. 10 (21), 10399–10420. https://doi.org/10.5194/acp-10-10399-2010.

Levy, R.C., Remer, L.A., Martins, J.V., Kaufman, Y.J., Plana-Fattori, A., Redemann, J., Wenny, B. (2005). Evaluation of the MODIS aerosol retrievals over ocean and land during CLAMS. J. Atmos. Sci. 62, 974 – 992.

Ma, Y., Li, Z., Li, Z., Xie, Y., Fu, Q., Li, D., Zhang, Y., Xu, H., Li, K. (2016). Validation of MODIS aerosol optical depth retrieval over mountains in Central China based on a sun-sky radiometer site of SONET. Remote Sens. 8 (2), 111. https://doi.org/10.3390/rs8020111.

Moorthy, K.K., Babu S.S., Satheesh, S.K., Srinivasan, J., Dutt, C.B.S. (2007). Dust absorption over the Great Indian Desert inferred using ground-based and satellite remote sensing. J. Geophys. Res. 112, D09206. Doi: 10.1029/2006JD007690.

More, S., Kumar, P.P., Gupta, P., Devara, P.C.S., Aher, G.R. (2013). Comparison of Aerosol Products Retrieved from AERONET, MICROTOPS and MODIS over a Tropical Urban City, Pune, India. Aerosol Air Qual. Res. 13, 107–121. Doi: 10.4209/aaqr.2012.04.0102.

Nichol, J.E., Bilal, M. (2016). Validation of MODIS 3 km Resolution Aerosol Optical Depth Retrievals Over Asia. Remote Sens. 8: 328. doi:10.3390/rs8040328

Ningombam, S.S., Bagare, S.P., Singh, R.B., Campanelli, M., Khatri, P., Dorjey, N. (2014). Calibration of a Sky radiometer (Prede) using observations obtained from Hanle and Merak high-altitude stations in Ladakh. Atmos. Res. 143, 118-128.

Pawar, G.V., Devara, P.C.S., Aher. G.R. (2015). Identification of Aerosol Types over an Urban Site Based on Air-Mass Trajectory Classification. Atmos. Res. 164–165, 142–155. Doi:10.1016/j.atmosres.2015.04.022.

Pawar, G.V., Devara, P.C.S., More, S.D., Kumar, P. P., Aher, G. R. (2012). Determination of Aerosol Characteristics and Direct Radiative Forcing at Pune. Aerosol Air Qual. Res. 12, 1166 – 1180. Doi:10.4209/aaqr.2011.09.0157.

Quenzel, H. (1970). Determination of Size Distribution of Atmospheric Aerosol Particles from spectral solar radiation measurements. J. Geophys. Res. 75(15), 2915–2921.

Rana, S., Kant, Y., Dadhwal, V. K. (2009). Diurnal and Seasonal Variation of Spectral Properties of Aerosols over Dehradun, India, Aerosol Air Qual. Res. 9(1), 32–49.

Ranjan, R.R., Joshi, H.P., Iyer, K.N. (2007). Spectral variation of total column aerosol optical depth over Rajkot: a tropical semi-arid Indian station. Aerosol Air Qual. Res. 7 (1), 33–45.

Sayer, A.M., Munchak, L.A., Hsu, N.C., Levy, R.C., Bettenhausen, C., Jeong, M.-J. (2014). MODIS Collection 6 aerosol products: Comparison between Aqua's e-Deep Blue, Dark Target, and "merged" data sets, and usage recommendations. J. Geophys. Res. Atmos. 119, 13965–13989. Doi: 10.1002/2014JD022453.

Schuster, G.L., Dubovik, O., Holben, B.N. (2006). Ångström Exponent and Bimodal Aerosol Size Distributions. J. Geophys. Res. 111, D07207. doi: 10.1029/2005JD006328.

Sharma, V., Ghosh, S., Bilal, M., Dey, S., Singh, S. (2021). Performance of MODIS C6.1 Dark Target and Deep Blue aerosol products in Delhi National Capital Region, India: Application for aerosol studies. Atmos. Pollut. Res. 12 (2021): 65–74. doi: 10.1016/j.apr.2021.01.023

Tian, X., Gao, Z. (2019). Validation and Accuracy Assessment of MODIS C6.1 Aerosol Products over the Heavy Aerosol Loading Area. Atmosphere. 10: 548. doi:10.3390/atmos10090548.

Varpe, S.R., Kolhe, A.R., Kutal, G.C., Pawar, G.V., Payra, S., Budhavant, K.B., Aher, G. R., Devara, P.C.S. (2018). Heterogeneity in aerosol characteristics at the semi-arid and island AERONET observing sites in India and Maldives. Int. J. Remote Sens. 39(19), 6137–6169. DOI: 10.1080/01431161.2018.1454622.

Vernekar, K.G., Mohan, Brij, Saxena, S., Patil, M.N. (1993). Characteristics of the atmospheric boundary layer over a tropical station as evidenced by tethered balloon observations. J. Appl. Meteorol. 32, 1426–1432.

Vijayakumar, K., Devara, P.C.S., Vijaya Bhaskara Rao S., Jayasankar, K.C. (2016). Dust aerosol characterization and transport features based on combined ground-based, satellite and model-simulated data. Aeolian Res. 21,75-85.

Wang, G., Yang, P., Zhou, X. (2017a). Identification of the driving forces of climate change using the longest instrumental temperature record. Sci. Rep. 7, 46091. Doi:10.1038/srep46091.

Wang, K., Sun, X., Zhou, Y., Zhang, C. (2017b). Validation of MODIS-Aqua Aerosol Products C051 and C006 over the Beijing-Tianjin-Hebei Region. Atmosphere. 8 (9), 172, Doi:10.3390/atmos8090172.

Tables

Table S1. Values of the factory generated and observed calibration constants (lnV_0) at each Microtops II channel with corresponding % deviation.

Channel	Wavelength (nm)	Factory lnV_0	Observed lnV_0	% Deviation of observed lnV_0
Channel 1	440	6.917	6.9167	–0.004
Channel 2	500	6.762	6.7582	–0.056
Channel 3	675	6.939	6.9598	+0.298
Channel 4	870	6.555	6.5573	+0.035
Channel 5	1020	7.010	7.0213	+0.161

Figures

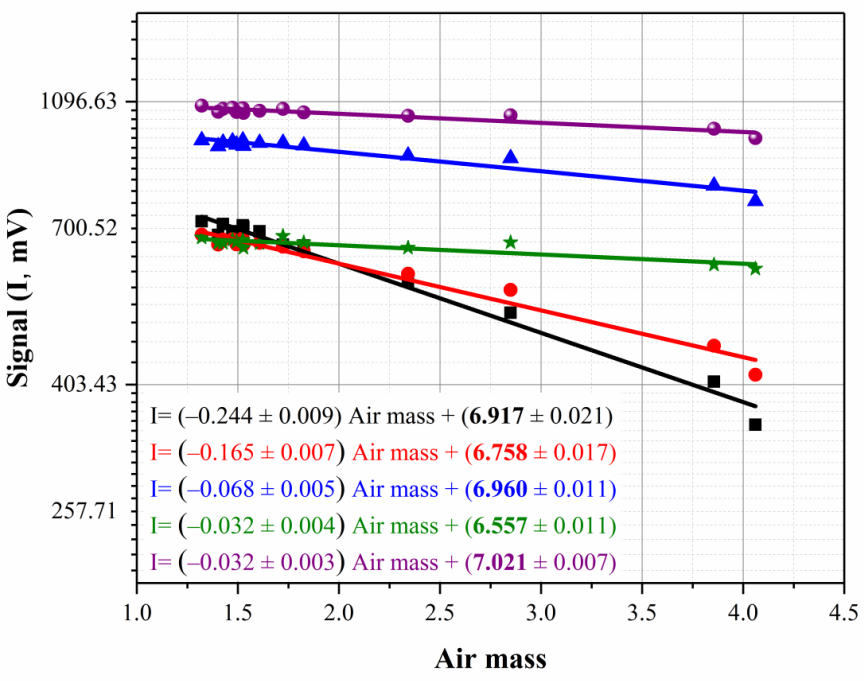

Fig. S1. The Langley plots, a plot of signal voltage $lnV(\lambda)$ against relative optical air mass, at 440, 500, 675, 870, and 1020 nm wavelengths displaying linear regression equations obtained at each wavelength and the respective Pearson's correlation coefficients (r).

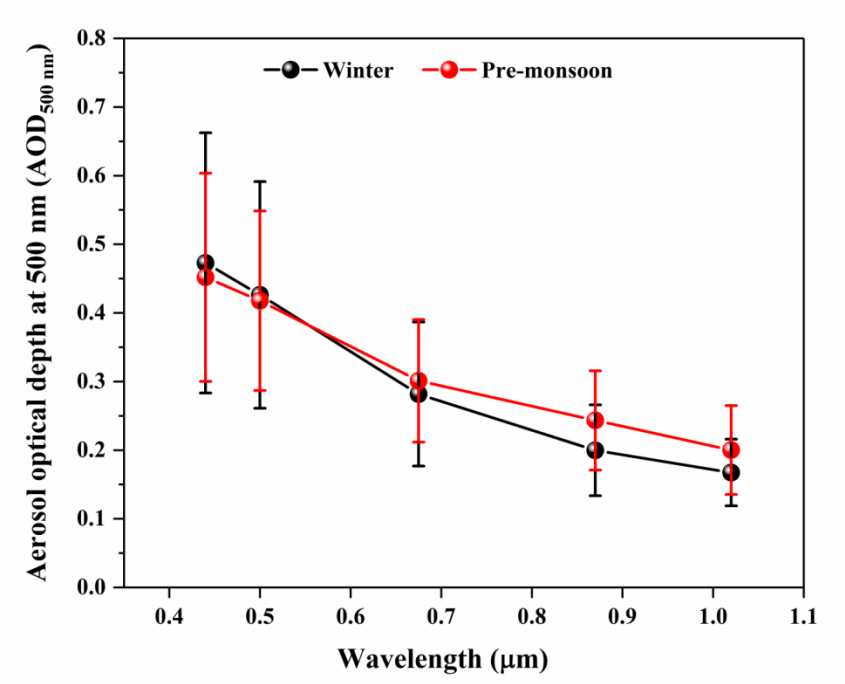

Fig. S2. Spectral variation of AOD obtained from Microtops-II Sun-photometer for winter (black sphere) and pre-monsoon (red sphere) seasons.

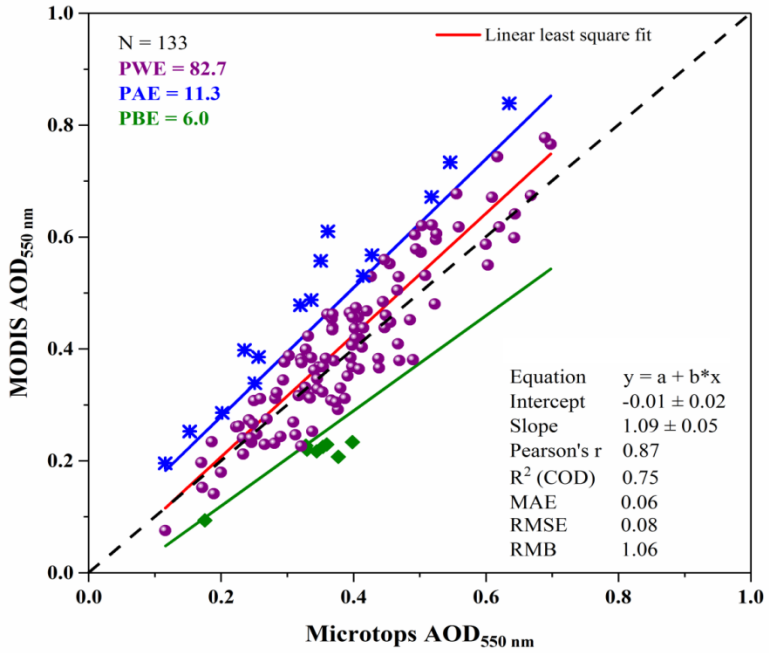

Fig. S3. 2-D scatter diagram of the collocated daily MODIS AOD_{500} nm (calculated) against Microtops-II Sunphotometer measured AOD_{500} nm at site AC-Ahmednagar for the period January 2016– May 2018.